Journal of Zhejiang University-SCIENCE A (Applied Physics & Engineering)
ISSN 1673-565X (Print); ISSN 1862-1775 (Online)
www.zju.edu.cn/jzus; www.springerlink.com
E-mail: jzus@zju.edu.cn

# Wind characteristics near the ground during typhoon Meari*

Xu WANG[1], Peng HUANG[†‡2], Xian-feng YU[1,3], Xin-rong WANG[2], Hai-ming LIU[1]

([1]*State Key Laboratory Breeding Base of Mountain Bridge and Tunnel Engineering, Chongqing Jiaotong University, Chongqing 400074, China*)

([2]*State Key Laboratory of Disaster Reduction in Civil Engineering, Tongji University, Shanghai 200092, China*)

([3]*State Key Laboratory of Subtropical Building Science, South China University of Technology, Guangzhou 510640, China*)

[†]E-mail: huangtju@tongji.edu.cn

Received Nov. 22, 2015; Revision accepted June 13, 2016; Crosschecked Dec. 12, 2016

**Abstract:** Wind speed and direction data during typhoon Meari were obtained from eight anemometers installed at heights of 10, 20, 30, and 40 m on a 40-m tower built in the Pudong area of Shanghai. Wind-turbulence characteristics, including wind-speed profile, turbulence integral scale, power spectra, correlations, and coherences were analyzed. Wind-speed profiles varied with time during the passage of Meari. Measured wind-speed profiles could be expressed well by both a power law and a log law. Turbulence integral scales for $u$, $v$, and $w$ components all increased with wind speed. The ratios of the turbulence scales among the turbulence components averaged for all 10-min data were 1:0.69:0.08 at 10 m, 1:0.61:0.09 at 20 m, and 1:0.65:0.13 at 40 m. The turbulence integral scales for the $u$ and $v$ components increased with average gust time, but the turbulence integral scale for the $w$ component remained almost constant when the gust duration was greater than 10 min. The decay factor of the coherence function increased slightly with wind speed, with average values for longitudinal and lateral dimensions of 14.3 and 11.3, respectively. The slope rates of the turbulence spectra in the inertial range were less than −5/3 at first, but gradually satisfied the Kolmogorov 5/3 law. The longitudinal wind-power fluctuation spectrum roughly fitted the von Karman spectrum, but slight deviations occurred in the high-frequency band for lateral and vertical wind-power fluctuation spectra.

**Key words:** Typhoon Meari; Field measurement; Turbulence integral scale; Decay factor; Power spectra
http://dx.doi.org/10.1631/jzus.A1500310 **CLC number:** TU317.2

## 1 Introduction

The coastal area of China experiences serious typhoons. Each year, several typhoons make landfall or pass by these regions, causing great economic losses and casualties. The losses from damage to low-rise buildings are particularly serious. To improve the typhoon resistance of buildings in these regions, thereby reducing losses during typhoons, wind data must first be obtained by means of field measurements so that the wind-field characteristics of typhoons can be described. Due to the high cost of this work, the long cycle of field-measurement studies, and the uncertainty of typhoons, only a few such studies have been carried out in China (Liu *et al.*, 2012; Wang *et al.*, 2013; 2015). To address this deficiency, a wind-engineering measurement base was co-established by Tongji University and the Pudong Airport Construction Group near Shanghai Pudong International Airport, China. It consists of a full-scale low-rise building and a 40-m anemometer tower. Its aim is to study wind characteristics near the ground and the wind-pressure characteristics of low-rise buildings during typhoons in China's southeast coastal area (Huang *et al.*, 2012).

Information related to typhoon Meari and the wind-engineering measurement base was published by Wang *et al.* (2012). In this study, we investigated

‡ Corresponding author

* Project supported by the National Natural Science Foundation of China (No. 51378396), the Open Project of Guangxi Key Laboratory of Disaster Prevention and Structural Safety (No. 2014ZDK005), and the Chongqing Postdoctoral Science Foundation (No. Xm2015066), China

ORCID: Xu WANG, http://orcid.org/0000-0001-5131-4016; Peng HUANG, http://orcid.org/0000-0002-5746-328X

turbulence characteristics including wind-speed profiles, turbulence integral scales, power spectra, correlations, and coherences during typhoon Meari, based on wind data collected from a 40-m tower equipped with eight ultrasonic and propeller anemometers at 10-, 20-, 30-, and 40-m levels. The results of this study provide a reference for typhoon-resistant design of structures in the eastern coastal areas of China.

## 2 Measurement procedures

### 2.1 Description of typhoon Meari

The fifth typhoon in 2011, typhoon Meari, was characterized by a wide area of influence, a fast forward motion, and small variations in intensity. The minimum distance between the observation site and the center of the typhoon was about 250 km. Winds of force 7–8 occurred along the Pudong coast of Shanghai and of force 6–8 in Shanghai City. Fig. 1 shows the observation location and a photo of the observation tower.

### 2.2 Experimental instruments and facilities

The lattice tower for measuring wind is 40 m tall and situated on a flat area close to the Yangtze River estuary, about 500 m from the east coast. Fig. 2 shows the terrain around the station in four directions. Fig. 3 shows a photo and a diagram of the arrangement of the anemometers. Three types of anemometers were used: 3D sonic anemometers (R.M. Young 81000), 2D sonic anemometers (R.M. Young 85106), and propeller anemometers (R.M. Young 05305V). The sampling frequency was 4 Hz, and the anemometers were installed at heights of 10, 20, 30, and 40 m, respectively, to record the wind speed and direction. The 0° wind direction corresponds to north. Positive wind directions were defined by clockwise rotation. The 3D sonic anemometers were used to select data for analysis, mainly because they can record wind-speed fluctuations in three dimensions. Data from the other types of anemometers were used only to supplement and correct these data. The distance from the anemometer to the tower body was far enough to avoid any significant effects on data acquisition, based on the results from previous computational fluid dynamics (CFD) numerical simulations.

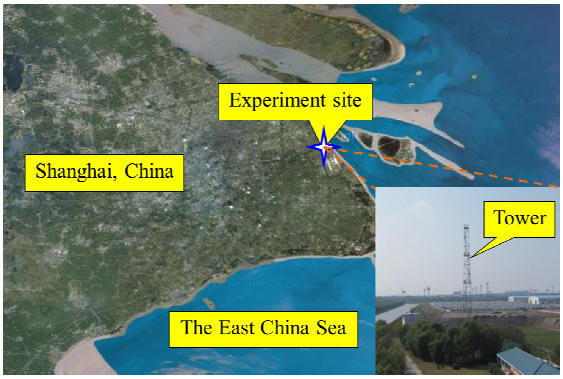


**Fig. 1 Observation location and a photo of the observation tower**

## 3 Wind characteristics of typhoon Meari near the ground

The recorded time of occurrence of typhoon Meari was from 14:00 on June 25, 2011 to 18:00 on June 26, 2011, a duration of 28 h. Based on the standard time interval in China, the data measurements were segmented into 10-min intervals; sample information for the data is listed in Table 1 (p.36). Fig. 4 (p.36) shows the variation in 10-min wind speed and wind direction with time. The mean wind speed generally increased with observation height, but the variation in mean wind direction with time was similar at different observation heights. The maximum mean wind speed occurred around 19:00 on June 25, 2011. The maximum mean wind speed, $U_{max}$, was 11.51 m/s at a height of 10 m and 15.05 m/s at a height of 40 m, and the lateral wind direction was about 17°.

## 4 Wind-speed profiles

### 4.1 Profile models

In general, most buildings are located in the atmospheric boundary layer. Therefore, it is important to describe wind-speed characteristics in that layer to achieve wind-resistant structural designs. The wind-speed profile is an important characteristic and is defined as the variation in mean wind speed with height over a certain averaging time. Several wind-speed profile models exist, including the power-law model (Davenport, 1960), the log-law model

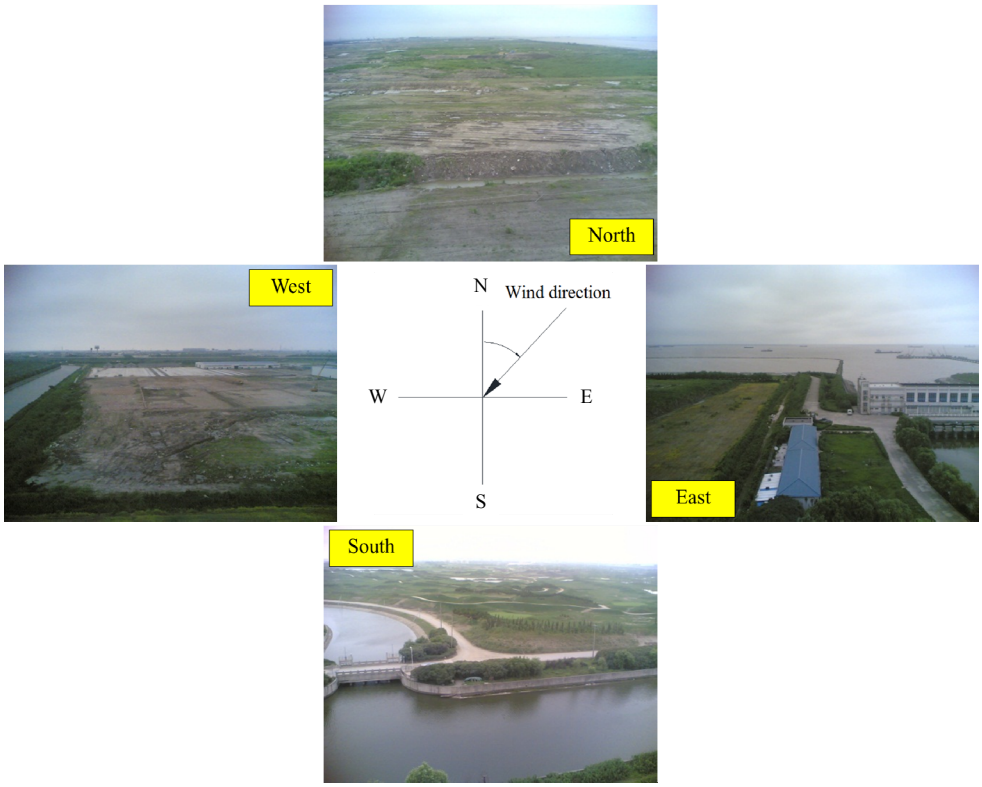


**Fig. 2 Photographs of the terrain around the observation station**

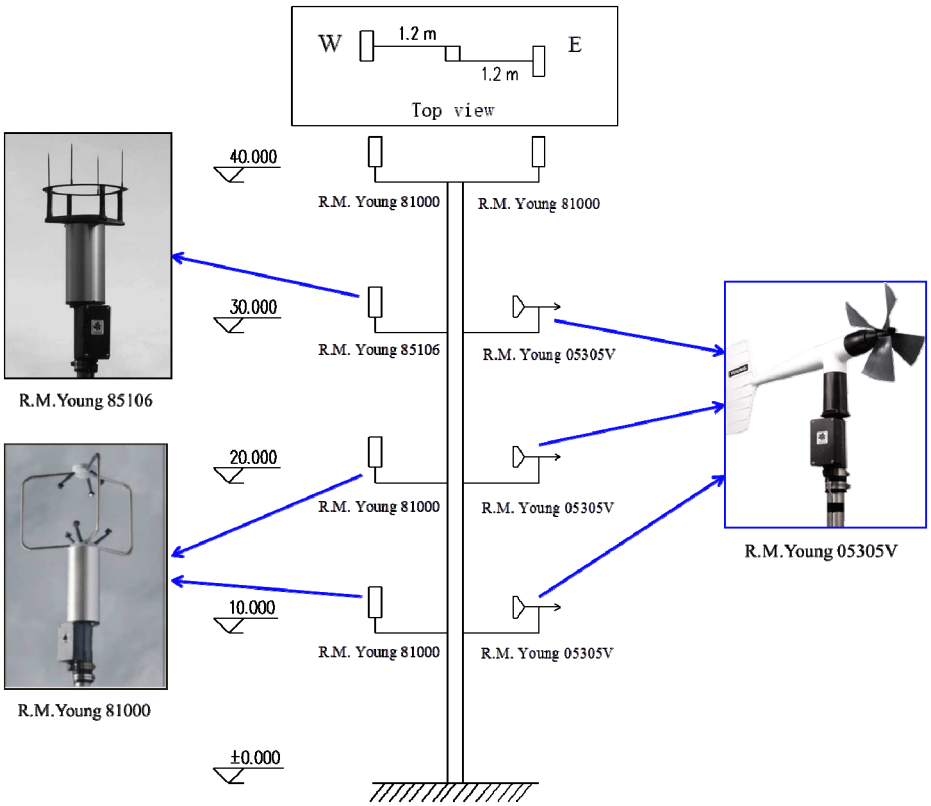


**Fig. 3 Arrangements of anemometers (unit: m)**

**Table 1 Measured data samples from the typhoon**

| Typhoon | Instrument | Height (m) | Sample number | $U_{max}$ (m/s) |
|---|---|---|---|---|
| Meari | Sonic anemometer | 10 | 160 | 11.51 |
| | | 20 | 160 | 13.08 |
| | | 30 | 160 | 14.67 |
| | | 40 | 160 | 15.04 |

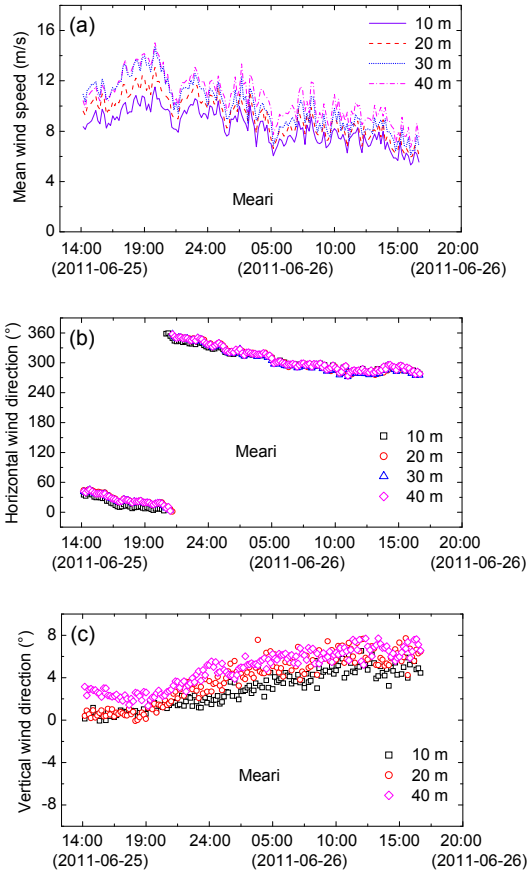


**Fig. 4 The 10-min mean wind speed and wind directions of typhoon Meari: (a) 10-min mean wind speed; (b) 10-min mean horizontal wind direction; (c) 10-min mean vertical wind direction**

(Davenport, 1960), and the Deaves-Harris model (Deaves and Harris, 1978; Deaves, 1981a; 1981b).

1. Power law: Based on statistical analysis of a large amount of data observations under various terrain conditions, Davenport (1960) pointed out that the power function can be used to describe the variation in mean wind velocity with height $z$, as follows:

$$\frac{U(z)}{U(z_{\mathrm{ref}})}=\left(\frac{z}{z_{\mathrm{ref}}}\right)^{\alpha}, \tag{1}$$

where $z_{\mathrm{ref}}$ is the reference height, $U(z_{\mathrm{ref}})$ is the mean velocity at the reference height, $U(z)$ is the mean velocity at height $z$, and $\alpha$ is the ground roughness exponent.

2. Log law: According to the asymptotic similarity considerations for a neutral atmospheric boundary layer, matching of the law of the wall with the velocity defect law in the overlap region, where both laws apply simultaneously, a wind speed profile at this point can be expressed as (Simiu and Scanlan, 1996; Tieleman, 2008):

$$U(z)=\frac{U_0^*}{k}\ln(z/z_0), \tag{2}$$

where $k$ is the Karman constant (here assumed to be 0.4), $U_0^*$ is the surface friction velocity, and $z_0$ is the surface roughness length. There is wide variability among the results from different experiments because of the heterogeneity of local air currents. In this study, $z_0$ was assumed to be 0.02 m, as recommended by the American Society of Civil Engineers (ASCE) standard ASCE/SEI 7-10 (ASCE, 2010), corresponding to roughness exposure C.

Friction velocity is an important index for measuring air friction and is widely used for quantitative analysis of turbulent diffusion in the whole atmospheric boundary layer. Two kinds of expressions have been used in earlier studies. Using the horizontal stress vector, several researchers have defined friction velocity as (Geernaert, 1988; Ly, 1993; Rotach, 1993; Patil, 2006)

$$U_{0(1)}^*=\left(\overline{u'w'}^2+\overline{v'w'}^2\right)^{1/4}, \tag{3}$$

where $u'$, $v'$, and $w'$ are the longitudinal, lateral, and vertical wind-fluctuation components, respectively.

Based on the hypothesis of Prandtl (1949), in which the Reynolds stress vector is parallel to the

mean wind direction, several researchers have defined the friction velocity as (Panofsky and Dutton, 1984; Grimmond *et al.*, 1998; Weber, 1999)

$$U^{*}_{0(2)}=\left(\left|\overline{u'w'}\right|\right)^{1/2}. \tag{4}$$

The variation in friction velocity calculated by Eq. (3) with mean wind speed was almost identical at different observation heights (Fig. 5). The friction velocity tended to increase with the increased mean wind speed at heights of 10 and 20 m, while at a height of 40 m, it showed only a small correlation with the mean wind speed. The mean friction velocity was 0.60 m/s at 10 m, 0.62 m/s at 20 m, and 0.58 m/s at 40 m. The friction velocity did not vary noticeably with height, which agrees with the conclusions of Li *et al.* (2010). For these reasons, friction velocity was taken as the average of three values (0.6 m/s) in log law expression.

## 4.2 Characteristics of the measured typhoon wind-velocity profile

Fig. 6 shows the mean wind-speed profiles over one-hour time periods, where the horizontal axis is the ratio of mean wind speed $U(z)$ to $U(10)$. Large variations were found among the profiles during the passage of the typhoon. In the beginning, the ratio of $U(40)$ to $U(10)$ was low, and even lower than the ratio of $U(30)$ to $U(10)$ in several 10-min time intervals. However, the ratio of $U(40)$ to $U(10)$ generally increased with time.

Fig. 7 shows mean wind-speed profiles by height at various 10-min time intervals in different wind-speed regions. In this study, $z_0$ was assumed to be 0.02 m, as recommended by ASCE/SEI 7-10 (ASCE, 2010), corresponding to roughness exposure C. The wind speed had a strong influence on the mean wind-speed profile when typhoon Meari was passing. The ratios of $U(z)$ to $U(10)$ at different wind-speed time intervals were similar when the wind speed was greater than 10 m/s, but deviated from the measured profiles when the wind speed was less than 10 m/s.

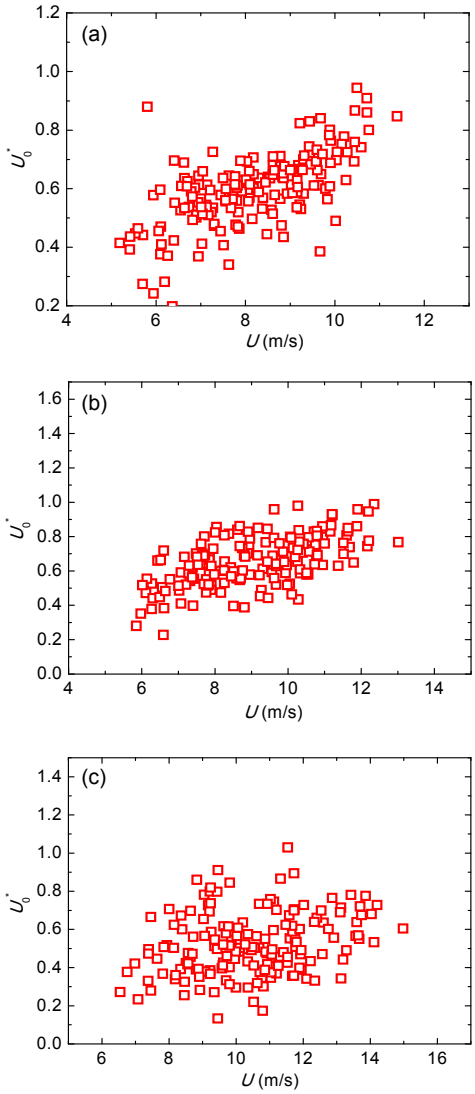


**Fig. 5 Variation in friction velocity with 10-min mean wind speed: (a) $z$=10 m; (b) $z$=20 m; (c) $z$=40 m**

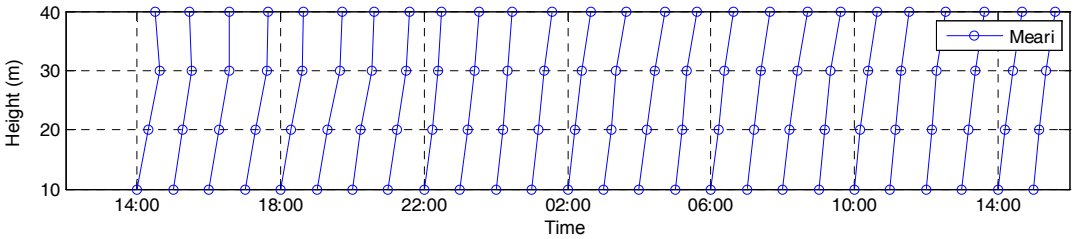


**Fig. 6 Mean wind-speed profiles over one-hour time intervals during typhoon Meari**

As a comparison between the measurements and the wind-speed profile models, Fig. 8 shows the mean wind-speed profiles at different wind-speed time intervals during typhoon Meari. The comparison was carried out between the measurements and the power-law and log-law models. It is evident that that power-law and log-law models can well express the measured wind profiles.

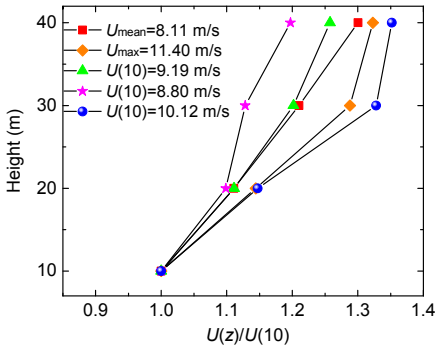


**Fig. 7 Measured mean wind-speed profiles**

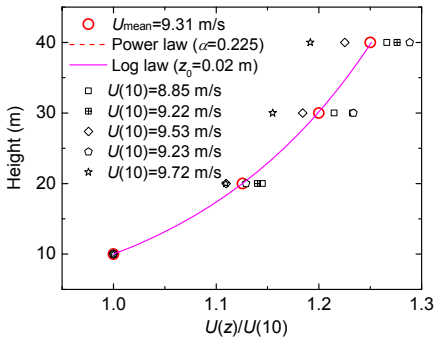


**Fig. 8 Comparison between the measured wind-speed profile and the profiles from the empirical models**

## 5 Turbulence integral scales

### 5.1 Method for calculating the turbulence integral scale

A turbulence integral scale is used to describe the size of scale eddies which occur frequently, play a leading role in turbulent eddies, and constitute a measure of mean turbulence scale in air currents. This is an important index which reflects the characteristics of a wind field. Evaluation of the energy contained in a turbulence scale is an important research topic in wind engineering. According to the definition of a turbulence integral scale (Simiu and Scanlan, 1996), it can be expressed as

$$L_i = \frac{1}{\sigma_i^2}\int_0^{\infty} R_{1,2}(x)\mathrm{d}x, \tag{5}$$

where $L_i$ is the turbulence integral scale of wind-speed fluctuations for the $i$ ($u$, $v$, or $w$) direction, $\sigma_i$ is the standard deviation of fluctuating wind speed in $i$ direction, and $R_{1,2}(x)$ is the cross-correlation function between measuring points 1 and 2.

Because of the difficulty of measuring many points synchronously in space, it is necessary to transform the spatial correlation into a time correlation using the Taylor hypothesis. The advantage of this method is that wind-speed fluctuations at many points in any space are transformed into an autocorrelation at a single point, and then integral calculations can be performed. The autocorrelation-function integral method based on the Taylor hypothesis is widely used and can be expressed as

$$L_i = \frac{U}{\sigma_i^2}\int_0^{\beta} R_i(\tau)\mathrm{d}\tau, \tag{6}$$

where $R_i(\tau)$ is the autocorrelation function for the $i$ direction, $\tau$ is the delay time, and $\beta$ is a parameter used when the autocorrelation coefficient drops to 0.05 (Flay and Stevenson, 1988).

### 5.2 Relationship between the turbulence integral scale and wind speed

Fig. 9 shows the variation in longitudinal ($L_u$), lateral ($L_v$), and vertical ($L_w$) turbulence integral scales with 10-min mean wind speeds at heights of 10, 20, and 40 m for a 10-min basic time interval. The turbulence integral scales of the 3D components increased with mean wind speed and their dispersion increased. The probability density distributions of the turbulence integral scales for 3D components are clearly asymmetrical, unlike standardized Gaussian distributions.

The ratios among longitudinal, lateral, and vertical turbulence integral scales obtained on the basis of field measurement by several researchers are shown in Table 2 (p.40), from which the results from different areas can be found. The measured longitudinal integral scale of Choi (1978) is obviously larger than those in this and other studies, and the results in this study are close to those of Cao *et al.* (2009) and Xiao *et al.* (2009). The ratios of the lateral and

longitudinal turbulence integral scales in this study are close to those of Xiao *et al.* (2009) and Song *et al.* (2012) and larger than those of other studies in Table 2. The ratios of vertical and longitudinal turbulence integral scales in our study agree well with the results of other studies (Table 2).

### 5.3 Turbulence integral scale profile

From Table 2, it is clear that the turbulence integral scale increases with observation height for a single typhoon. Empirical expressions for the variation of longitudinal turbulence integral scale with

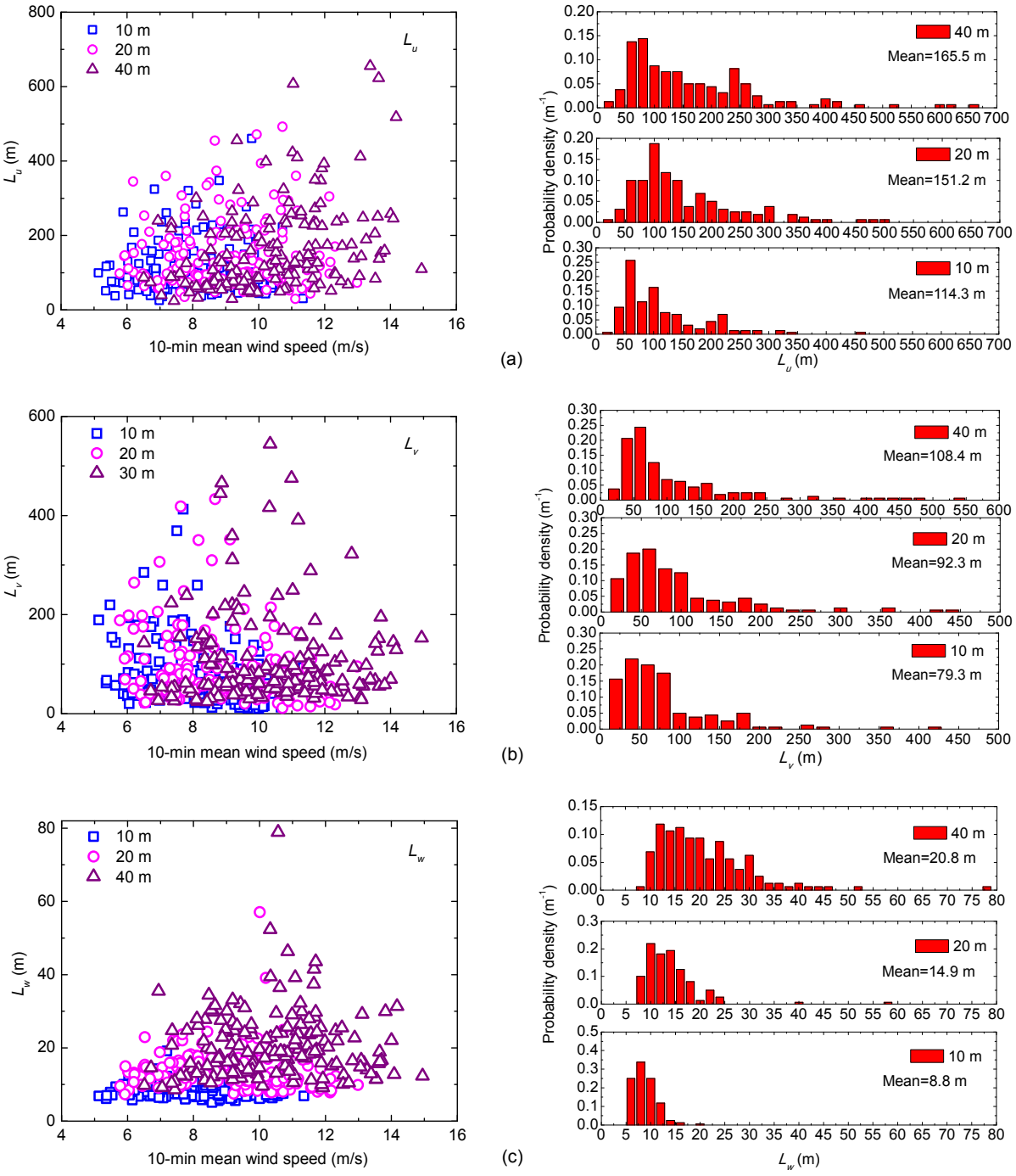


**Fig. 9 Variation in turbulence integral scales with wind speed and probability density of the turbulence integral scale**
(a) Longitudinal; (b) Lateral; (c) Vertical

**Table 2 Ratios of turbulence integral scales among the turbulence components**

| Reference | Typhoon name | Experimental environment | | $L_u$:$L_v$:$L_w$ ($L_u$ (m)) |
|---|---|---|---|---|
| | | Terrain | Height (m) | |
| This study | "Meari" (2011) | Seaside, Shanghai, China | 40 | 1:0.65:0.13 (165.5) |
| | | | 20 | 1:0.61:0.09 (151.2) |
| | | | 10 | 1:0.69:0.08 (114.3) |
| Choi, 1978 | "Freda" (1971) | Seaside, Hong Kong, China | 59.4 | 1:0.17:0.15 (532) |
| | | | 42.9 | 1:0.17: – (423) |
| | | | 27.8 | 1:0.20: – (312) |
| | | | 12.8 | 1:0.13:0.22 (216) |
| Kato *et al*., 1992 | "8922", "9011" | City center, Tokyo, Japan | 56 | 1:0.33:0.17 (58) |
| | | | 86 | 1:0.50:0.17 (133) |
| Xiao *et al*., 2009 | "Chanzhu" (2006) | Red Bay, China | 10 | 1:0.63:0.08 (97.8) |
| | | | 30 | 1:0.74: – (193.4) |
| Cao *et al*., 2009 | "Maemi" (2003) | Seaside, Miyakojima, Japan | 15 | 1:0.42:0.18 (100) |
| Hui *et al*., 2009 | "Imbudo", "Dujuan", "Krovanh" (2003); "Kompasu" (2004) | Seaside, Hong Kong, China | 50 | SW: 1:0.43:0.1 (199) NE: 1:0.36:0.08 (272) |
| Song *et al*., 2012 | "Hagupit" | Guangdong, China | 60 | 1:0.66:0.16 (313) |

height have been included in the wind-load standards and codes of many countries, but not China.

Fig. 10a shows the variation of the measured longitudinal turbulence integral scale with height. For comparison, the longitudinal empirical results from many other countries are also given. The longitudinal result stipulated in ASCE (2010) is the largest and those in the Architectural Institute of Japan (AIJ, 2004) and European (BSI, 2004) specifications are smaller at the same height. The measured results are close to the result stipulated in ASCE (2010) at 10 m height and larger than those stipulated in all specifications when the height was greater than 10 m. For the purposes of engineering application and of providing a reference for wind-resistant design, the formula $L(z)=a(z/10)^b$ has been used to fit the relationship between measured longitudinal turbulence integral scale and height. Fig. 10a shows the fitted curve, and the fitting parameters $a$ and $b$ are shown in Table 3.

Until now, there have been no empirical formulas for lateral and vertical turbulence integral scales in national specifications, and there have been few related studies. Three-dimensional turbulence integral scale profiles of typhoon Freda were measured in Hong Kong, China and fitted by Choi (1978). Based on the data measurements in this study, a comparison between the earlier results and the observed variation

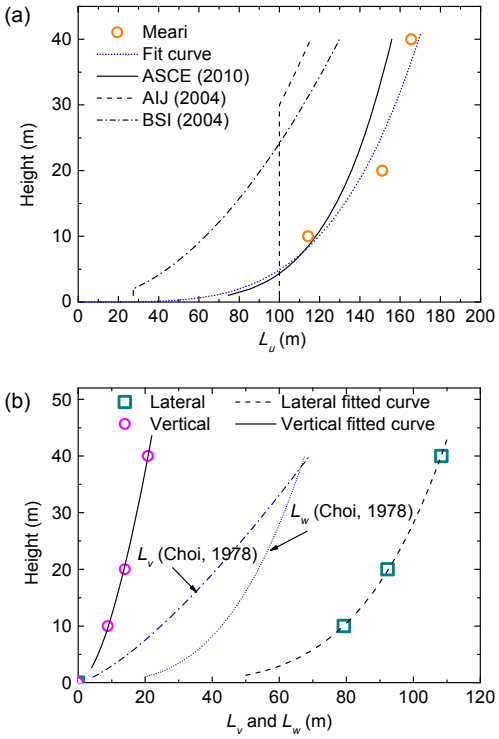


**Fig. 10 Variation of turbulence integral scale with observation height**

of lateral and vertical turbulence integral scales with height is shown in Fig. 10b, and the fitting parameters are shown in Table 3. Compared with the integral

scale profiles of typhoon Freda measured by Choi (1978), the measured values of $L_v$ are smaller, and the values of $L_w$ are larger in this study.

**Table 3 Fitting parameters for turbulence integral scale profiles ($L_i$=$a$($z$/10)$^b$) of typhoon Meari**

| Fitting parameter | $a$ | $b$ |
|---|---|---|
| $L_u^x$ | 119.54 | 0.25 |
| $L_v^x$ | 78.45 | 0.23 |
| $L_w^x$ | 9.21 | 0.61 |

### 5.4 Relationship between turbulence integral scale and time interval

Previous studies have shown that the turbulence integral scale is related not only to measured height, but also to the selected time interval, $T$ (Yu and Chowdhury, 2009). Because there are large variations in the basic time interval stipulated in the specifications of various countries, simple comparisons will lead to large errors, which are bad for design practice. Based on measured wind-speed fluctuation values for typhoon Meari at 10-, 20-, and 40-m heights, Fig. 11 shows the variation of the turbulence integral scales of the 3D components with time interval. The longitudinal and lateral turbulence integral scales at different heights increase with average gust time, in accordance with the results of Yu and Chowdhury (2009) and Schroeder and Smith (2003). Comparing our results with those of Yu and Chowdhury (2009) for many typhoons at a height of 10 m, the measured lateral integral scale is close to the result for hurricane Lili in wide uplands. The longitudinal integral scale can be greater than the lateral value if it increases to a certain extent with time interval. Unlike the longitudinal and lateral scales, the vertical turbulence integral scales at various heights increase with time interval and remain constant when time interval is not less than 10 min. The main reason for this is that the vertical wind characteristic is different from longitudinal and lateral characteristics.

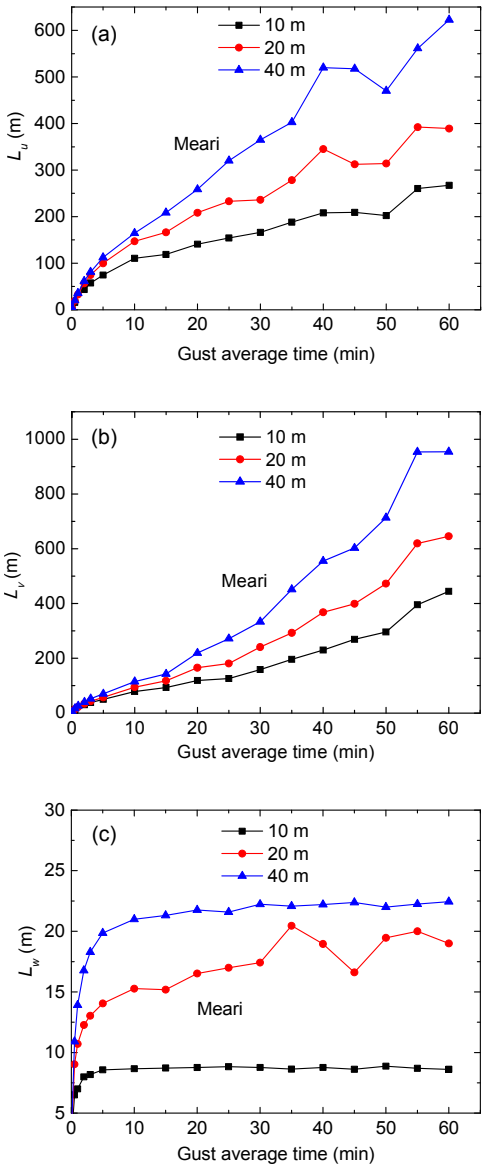


**Fig. 11 Variation of turbulence integral scale with average gust time: (a) longitudinal; (b) lateral; (c) vertical**

## 6 Correlation and coherence

### 6.1 Correlation analysis

Autocorrelation describes the correlation of two dependent values of a time series at different moments. If $X(t)$ is a time series, the correlation function can be expressed as

$$R_{XX}(t_1, t_2) = E\left[X(t_1)X(t_2)\right], \tag{7}$$

where $R_{XX}$ is the autocorrelation function.

If $X(t)$ is a stationary random process, the correlation function can be expressed as

$$R_{XX}(\tau) = E\left[X(t)X(t+\tau)\right]. \tag{8}$$

The cross-correlation function describes the correlation intensity of random signals $X(t)$ and $Y(t)$ at any two different times. It can be expressed as

$$C_{R(ij)}=\frac{R_{ij}(0)}{\sqrt{R_{ii}(0)}\sqrt{R_{jj}(0)}}, \tag{9}$$

where $C_{R(ij)}$ is the cross-correlation coefficient of wind-speed fluctuations for components $i$ and $j$, $R_{ij}$ is the cross-correlation function of wind-speed fluctuations for components $i$ and $j$, and $R_{ii}$ and $R_{jj}$ are autocorrelation functions of wind-speed fluctuation components in the $i$ and $j$ directions, respectively.

Fig. 12 shows the variation of the autocorrelation coefficient of longitudinal wind-speed fluctuations with height. The curve is the average value of the measured autocorrelation coefficients of wind-speed fluctuations over various 10-min time intervals. To compare our results with published data, the curves of the autocorrelation coefficient are included in Fig. 12. The autocorrelation coefficient decreases markedly with lag $\tau$ and the rate of change varies with height. The curves obtained from the hurricanes Isodore, Lili (Yu and Chowdhury, 2009), and Bonnie (Schroeder and Smith, 2003) decay more gently than that presented in this study. The time intervals for the hurricanes Isodore, Lili, and Bonnie were selected as 60, 60, and 15 min, respectively, which are longer than the interval used in this study. As most current studies (Schroeder and Smith, 2003; Yu and Chowdhury, 2009) show that the decay rate increases as the time interval decreases, a more rapid decrease of the curve was seen in our study.

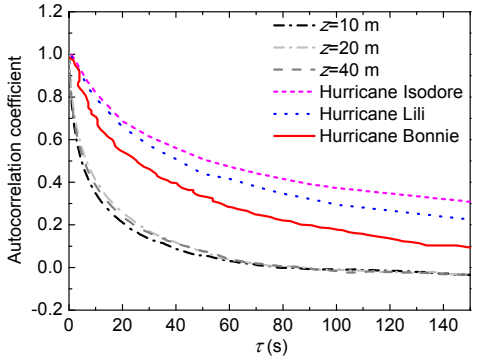


**Fig. 12 Autocorrelation coefficients for the longitudinal component at different heights**

Fig. 13 shows the variation in the minimum and maximum cross-correlation coefficients of wind-speed fluctuations for 3D components with time at heights of 10 and 20 m. In Fig. 13a, it is apparent that $C_{R(uu)}\geq C_{R(vv)}\geq C_{R(ww)}$ at heights of 10 and 20 m over 10-min time intervals, that the three values increase with time, and that $C_{R(ww)}$ has a tendency to increase. In Fig. 13b, it is clear that $C_{R(ww)}\geq C_{R(vv)}\geq C_{R(uu)}$ and that $C_{R(uu)}$ and $C_{R(vv)}$ decrease with time, but that $C_{R(ww)}$ increases with time before 22:00 on June 25, after which it varies insignificantly with time.

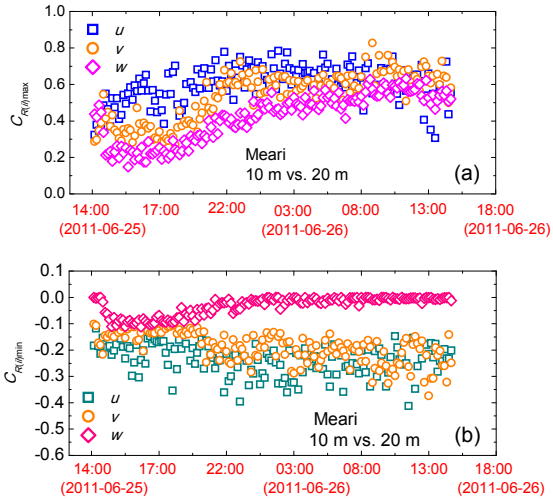


**Fig. 13 Variation of the maximum (a) and minimum (b) values of cross-correlation coefficients with time**

The variations in cross-correlation coefficients among 3D components of wind-speed fluctuations with mean wind speed are shown in Figs. 14 and 15. The coefficient $C_{R(uw)}$ at the height of 10 m was −0.23 during the typhoon Meari, which is larger than Cao *et al.* (2009)'s result. At a height of 40 m, the coefficient was −0.14, which shows that the vertical shearing action at a height of 40 m was less than that at 10 m. At both 10 and 40 m, the averages of $C_{R(uv)}$ and $C_{R(vw)}$ oscillated around zero.

## 6.2 Coherence analysis

In contrast to the correlation coefficient, the coherence coefficient describes the correlation intensity among signals in the frequency domain. Davenport (1968) assumed that the coherence coefficient followed the exponential function form and developed an empirical expression for the coherence

coefficient for wind-speed fluctuation components, which can be expressed as

$$\mathrm{Coh}(f)=\exp\left[-\frac{f}{U}\left(C_z^2\Delta z^2+C_y^2\Delta y^2\right)^{1/2}\right], \qquad (10)$$

where Coh is the coherence coefficient, $f$ is the frequency, $C_y$ and $C_z$ are the exponential decay coefficients in the lateral and vertical directions, respectively, and $\Delta y$ and $\Delta z$ are the distances between two points measured in the lateral and vertical directions, respectively.

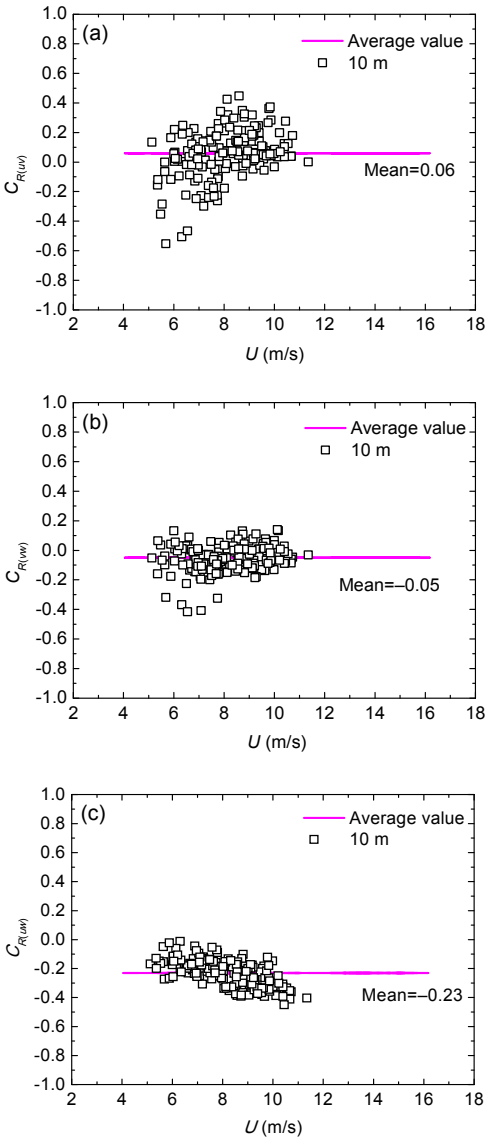


**Fig. 14 Variation in cross-correlation coefficients with wind speed at 10 m height: (a) $C_{R(uv)}$; (b) $C_{R(vw)}$; (c) $C_{R(uw)}$**

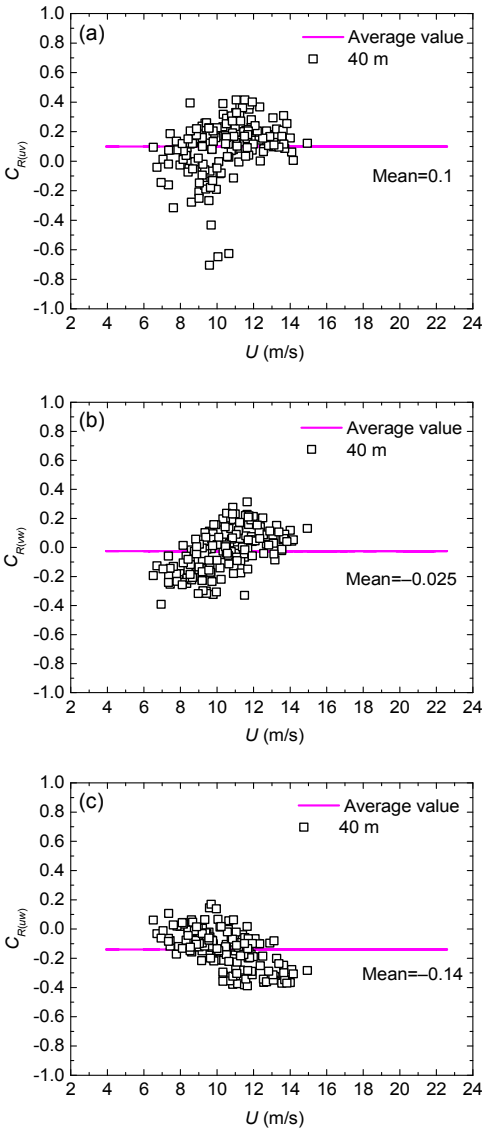


**Fig. 15 Variation in cross-correlation coefficients with wind speed at 40 m height: (a) $C_{R(uv)}$; (b) $C_{R(vw)}$; (c) $C_{R(uw)}$**

Eq. (10) can be simplified as

$$\mathrm{Coh}(f)=\exp\left(-C_z\frac{f\Delta z}{U}\right). \qquad (11)$$

Because the variation of the measured decay coefficient with wind speed is discrete, it is dealt with in this study by using mean values (Fig. 16). The exponential decay coefficients of wind-speed fluctuations of longitudinal and lateral components with mean wind speed are insignificant, although fluctuations did occur. The averages of the longitudinal and lateral components were 14.3 and 11.3, respectively,

which are larger than those of Cao *et al.* (2009) and Hui *et al*. (2009). Fig. 17 shows the curves of the coherence coefficients of wind-speed fluctuations of longitudinal and lateral components over different wind-speed time intervals. They follow an exponential trend. Eq. (11) describes well the coherence properties of wind-speed fluctuation components at different heights in these experiments.

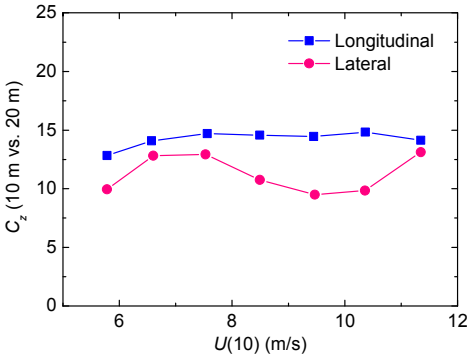


**Fig. 16 Variation of exponential decay coefficients with wind speed**

## 7 Power spectral density of wind-speed fluctuations

### 7.1 Definition of the auto-power spectrum

Based on the Kolmogorov principle, many power-spectrum function expressions for wind fluctuations have been developed, including the von Karman, Davenport, Simiu, Kaimal, and Harris spectra. Based on the results of field and wind-tunnel measurements (Shiau, 2000; Cao *et al.*, 2009; Xiao *et al.*, 2009), it is apparent that the von Karman type spectrum (von Karman, 1948) can accurately express the spectral characteristics of wind-speed fluctuations. This spectrum can be expressed as follows.

For longitudinal direction,

$$\frac{nS_u(n)}{\sigma_u^2}=\frac{4f}{(1+70.8f^2)^{5/6}}, \tag{12}$$

and for lateral and vertical directions,

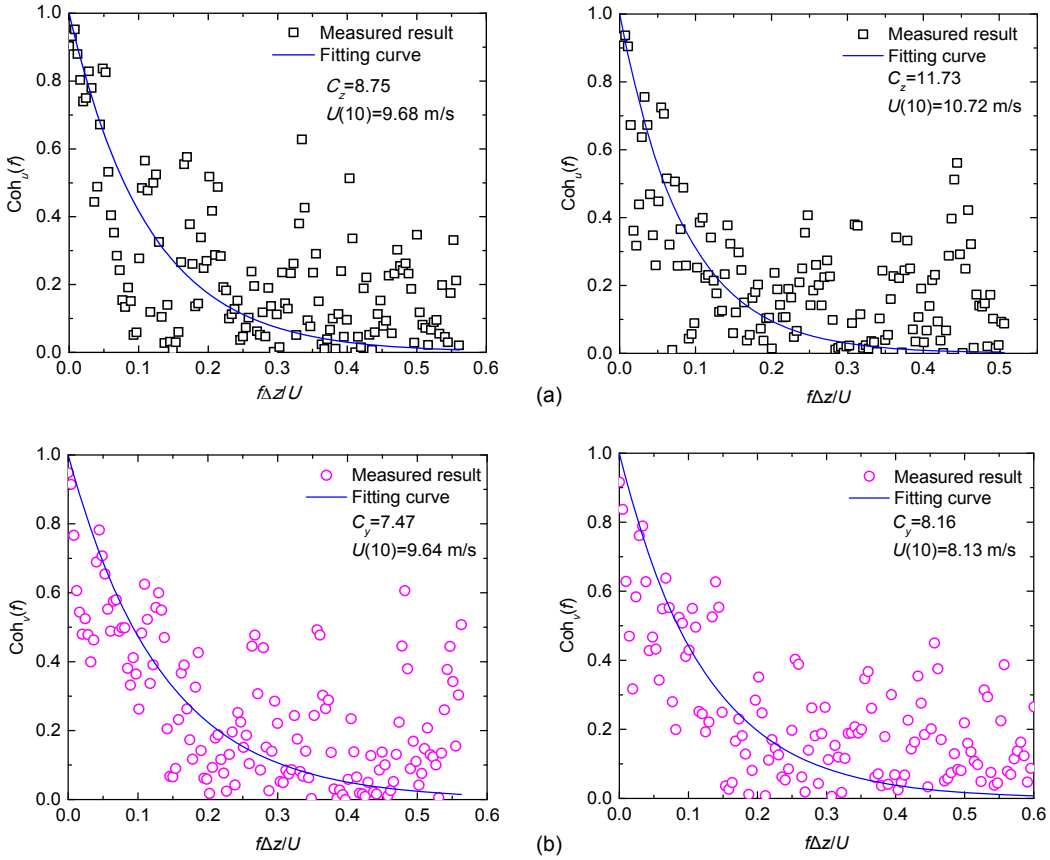


**Fig. 17 Comparison between coherence functions and measured results: (a) longitudinal; (b) lateral**

$$\frac{nS_i(n)}{\sigma_i^2}=\frac{4f(1+755.2f^2)}{(1+283.2f^2)^{11/6}},\quad i=v,w, \tag{13}$$

where $S_i(n)$ ($i$=$u$, $v$, $w$) is the power-spectrum function for the $i$ direction, $f$ denotes the reduced frequency derived as $f$=$nz$/$U(z)$, and $\sigma_i$ is the standard deviation of the wind-component fluctuations.

### 7.2 Analysis of measured spectra

Fig. 18 shows the power-spectrum density curves of the 3D velocity components ($u$, $v$, $w$) over different 10-min time intervals at heights of 10 and 20 m during the passage of typhoon Meari. Energy decays at high frequencies but remains almost constant at low frequencies. Similar to the results of Song *et al.* (2012), the power-spectrum distribution slope of the turbulent components in the inertial region transformed generally over time from being less than −5/3 to satisfying the Kolmogorov law.

Fig. 19 shows the power spectra of the 3D velocity components over 10 min at heights of 10 and 40 m, as well as the corresponding Karman empirical spectra. The measured power spectra for the longitudinal component agree well with the Karman empirical spectrum. However, those of the lateral and vertical velocity components deviate from the Karman empirical spectrum at high frequencies, in agreement with the conclusions of Xu and Zhan (2001).

## 8 Conclusions

Wind characteristics of typhoon Meari, including the wind-speed profile, turbulence integral scale, power spectra, correlations, and coherences at heights of 10, 20, 30, and 40 m, were analyzed on the basis of 10-min wind-speed samples. The major results can be summarized as follows:

1. The variation in friction velocity with height was insignificant, with values at heights of 10, 20, and 40 m of 0.60, 0.62, and 0.58 m/s, respectively. This result agrees well with the conclusions of Li *et al.* (2010). Measured wind-speed profiles can be expressed well by both the power law and the log law.

2. The autocorrelation coefficient decreased markedly with a lag and the rate of change varied with height. The curves obtained from the hurricanes Isodore, Lili, and Bonnie decayed more gently than the curve presented in this paper for the different time intervals. The cross-correlation coefficients of wind-speed components and the decay factor of the coherence function for longitudinal and lateral components increased slightly with wind speed.

3. The turbulence integral scale increased with mean wind speed, and the ratios of turbulence integral scale among the turbulence components averaged over all 10-min data were 1:0.69:0.08, 1:0.61:0.09, and 1:0.65:0.13 at 10, 20, and 40 m, respectively. The

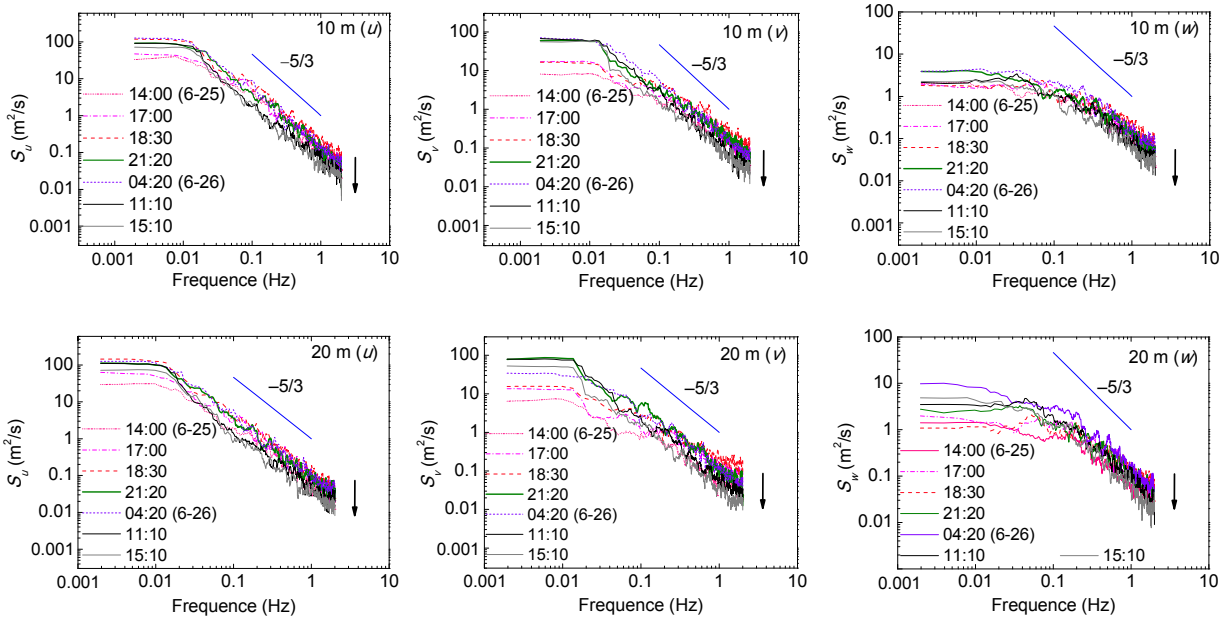


**Fig. 18 Power spectra of three wind-speed components at different times**

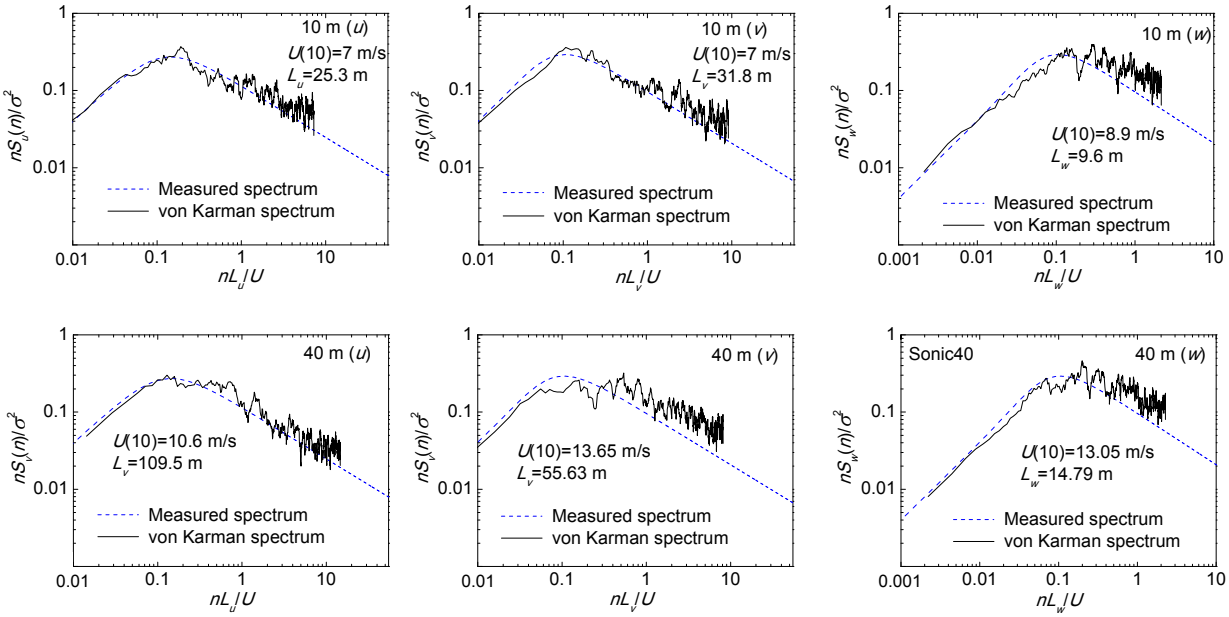


**Fig. 19 Comparison between the measured power spectra and von Karman spectra**

ratio of lateral and longitudinal turbulence integral scales in this study was close to those of Xiao *et al.* (2009) and Song *et al.* (2012) and larger than those of other studies. The ratio of vertical and longitudinal turbulence integral scales agreed well with the results of studies shown in Table 2.

4. The slope of the rates of turbulence spectra in the inertial range was less than −5/3 at first, but gradually came to satisfy the Kolmogorov 5/3 law over time during typhoon Meari. The longitudinal wind-power fluctuation spectrum can be roughly fitted using the von Karman spectrum, but there is a slight deviation in the high-frequency band for the lateral and vertical wind-power fluctuation spectra.

## References

AIJ (Architectural Institute of Japan), 2004. AIJ 2004 Recommendations for Loads on Buildings. AIJ, Tokyo, Japan.

ASCE (American Society of Civil Engineers), 2010. Minimum Design Loads for Buildings and Other Structures, ASCE/SEI 7-10. ASCE, Reston, VA, USA.

BSI (British Standards Institution), 2004. "Structural Eurocodes", Eurocode 1: Actions on Structures-General Actions-Part 1-4: Wind actions, Technical Committee CEN/TC250. BSI, London, UK.

Cao, S.Y., Tamura, Y., Kikuchi, N., *et al.*, 2009. Wind characteristics of a strong typhoon. *Journal of Wind Engineering and Industrial Aerodynamics*, **97**(1):11-21. http://dx.doi.org/10.1016/j.jweia.2008.10.002

Choi, E.C.C., 1978. Characteristics of typhoons over the South China Sea. *Journal of Wind Engineering and Industrial Aerodynamics*, **3**(4):353-365. http://dx.doi.org/10.1016/0167-6105(78)90038-7

Davenport, A.G., 1960. Rationale for determining design wind velocities. *ASCE Journal of the Structural Division*, **86**(5):39-68.

Davenport, A.G., 1968. The dependence of wind load on meteorological parameters. *In*: Wind Effects on Building and Structures. University of Toronto Press, Toronto, Canada, p.19-82.

Deaves, D.M., 1981a. Computations of wind flow over changes in surface roughness. *Journal of Wind Engineering and Industrial Aerodynamics*, **7**(1):65-94. http://dx.doi.org/10.1016/0167-6105(81)90068-4

Deaves, D.M., 1981b. Terrain dependence of longitudinal R.M.S. velocities in the neutral atmosphere. *Journal of Wind Engineering and Industrial Aerodynamics*, **8**(3):259-274. http://dx.doi.org/10.1016/0167-6105(81)90025-8

Deaves, D.M., Harris, R.I., 1978. A Mathematical Model of the Structure of Strong Winds. Technical Report, Construction Industry Research and Information Association, London, UK.

Flay, G.J., Stevenson, D.C., 1988. Integral length scales in strong winds below 20 m. *Journal of Wind Engineering and Industrial Aerodynamics*, **28**(1-3):21-30. http://dx.doi.org/10.1016/0167-6105(88)90098-0

Geernaert, G.L., 1988. Measurements of the angle between the wind vector and wind stress vector in the surface layer

over the North Sea. *Journal of Geophysical Research: Oceans*, **93**(C7):8215-8220. http://dx.doi.org/10.1029/JC093iC07p08215

Grimmond, C.S.B., King, T.S., Roth, M., *et al*., 1998. Aerodynamic roughness of urban areas derived from wind observations. *Boundary-Layer Meteorology*, **89**(1):1-24. http://dx.doi.org/10.1023/A:1001525622213

Huang, P., Wang, X., Gu, M., 2012. Field experiments for wind loads on a low-rise building with adjustable pitch. *International Journal of Distributed Sensor Networks*, **2012**: 1-10. http://dx.doi.org/10.1155/2012/451879

Hui, M.C.H., Larsen, A., Xiang, H.F., 2009. Wind turbulence characteristics study at the Stonecutters Bridge site: part II—wind power spectra, integral length scales and coherences. *Journal of Wind Engineering and Industrial Aerodynamics*, **97**(1):48-59. http://dx.doi.org/10.1016/j.jweia.2008.11.003

Kato, N., Ohkuma, T., Kim, J.R., *et al.*, 1992. Full scale measurements of wind speed in two urban areas using an ultrasonic anemometer. *Journal of Wind Engineering and Industrial Aerodynamics*, **41**(1-3):67-78. http://dx.doi.org/10.1016/0167-6105(92)90394-P

Li, Q.S., Zhi, L., Hu, F., 2010. Boundary layer wind structure from observations on a 325 m tower. *Journal of Wind Engineering and Industrial Aerodynamics*, **98**(12):818-832. http://dx.doi.org/10.1016/j.jweia.2010.08.001

Liu, M., Liao, H., Li, M., *et al.*, 2012. Long-term field measurement and analysis of the natural wind characteristics at the site of Xi-hou-men Bridge. *Journal of Zhejiang University-SCIENCE A (Applied Physics & Engineering)*, **13**(3):197-207. http://dx.doi.org/10.1631/jzus.A1100178

Ly, L.N., 1993. Effects of the angle between wind stress and wind velocity vectors on the aerodynamic drag coefficient at the air-sea interface. *Journal of Physical Oceanography*, **23**(1):159-163. http://dx.doi.org/10.1175/1520-0485(1993)023<0159:EOTABW>2.0.CO;2

Panofsky, H.A., Dutton, J.A., 1984. Atmospheric Turbulence: Models and Methods for Engineering Applications. John Wiley & Sons, Inc., New York, USA, p.62-63.

Patil, M.N., 2006. Aerodynamic drag coefficient and roughness length for three seasons over a tropical western Indian station. *Atmospheric Research*, **80**(4):280-293. http://dx.doi.org/10.1016/j.atmosres.2005.10.005

Prandtl, L., 1949. Führer durch die Strömungslehre. Friedrich Vieweg & Sohn, Braunschweig, Germany (in German).

Rotach, M.W., 1993. Turbulence close to a rough urban surface part I: Reynolds stress. *Boundary-Layer Meteorolgy*, **65**(1-2):1-28. http://dx.doi.org/10.1007/BF00708816

Schroeder, J.L., Smith, D.A., 2003. Hurricane Bonnie wind flow characteristics as determined from WEMITE. *Journal of Wind Engineering and Industrial Aerodynamics*, **91**(6):767-789. http://dx.doi.org/10.1016/S0167-6105(02)00475-0

Shiau, B.S., 2000. Velocity spectra and turbulence statistics at the northeastern coast of Taiwan under high-wind condition. *Journal of Wind Engineering and Industrial Aerodynamics*, **88**(2-3):139-151. http://dx.doi.org/10.1016/S0167-6105(00)00045-3

Simiu, E., Scanlan, R.H., 1996. Wind Effects on Structures —Fundamentals and Applications to Design. John Wiley & Sons, Inc., USA.

Song, L.L., Li, Q.S., Chen, W.C., *et al.*, 2012. Wind characteristics of a strong typhoon in marine surface boundary layer. *Wind and Structures*, **15**(1):1-15. http://dx.doi.org/10.12989/was.2012.15.1.001

Tieleman, H.W., 2008. Strong wind observations in the atmospheric surface layer. *Journal of Wind Engineering and Industrial Aerodynamics*, **96**(1):41-77. http://dx.doi.org/10.1016/j.jweia.2007.03.003

von Karman, T., 1948. Progress in the statistical theory of turbulence. *Proceedings of the National Academy of Sciences of the United States of America*, **34**(11):530-539.

Wang, H., Li, A., Niu, J., *et al.*, 2013. Long-term monitoring of wind characteristics at Sutong Bridge site. *Journal of Wind Engineering and Industrial Aerodynamics*, **115**:39-47. http://dx.doi.org/10.1016/j.jweia.2013.01.006

Wang, H., Guo, T., Tao, T.Y., *et al.*, 2015. Study on wind characteristics of Runyang Suspension Bridge based on long-term monitored data. *International Journal of Structural Stability and Dynamics*, **16**(4):1640019. http://dx.doi.org/10.1142/s0219455416400198

Wang, X., Huang, P., Gu, M., 2012. Field investigation on wind loads of a low building with adjustable roof pitch near sea. *Journal of Vibration and Shock*, **31**(20):84-89 (in Chinese).

Weber, R.O., 1999. Remarks on the definition and estimation of friction velocity. *Boundary-Layer Meteorology*, **93**(2): 197-209. http://dx.doi.org/10.1023/A:1002043826623

Xiao, Y.Q., Li, L.X., Song, L.L., 2009. Study on typhoon wind characteristics based on field measurements. The Seventh Asia-Pacific Conference on Wind Engineering.

Xu, Y.L., Zhan, S., 2001. Field measurements of Di Wang Tower during Typhoon York. *Journal of Wind Engineering and Industrial Aerodynamics*, **89**(1):73-93. http://dx.doi.org/10.1016/S0167-6105(00)00029-5

Yu, B., Chowdhury, A.G., 2009. Gust factors and turbulence intensities for the tropical cyclone environment. *Journal of Applied Meteorology and Climatology*, **48**(3):534-552. http://dx.doi.org/10.1175/2008JAMC1906.1

## 中文概要

**题　目：** 台风“米雷”近地层风特性实测研究

**目　的：** 对台风“米雷”作用下上海浦东近海岸边近地风特性进行全场监测记录，获得 10 m、20 m、30 m 和 40 m 高度处的风速实测数据，以研究台风过程中的平均风速风向、湍流度、阵风因子、湍流积分尺度和脉动风速功率谱等近地风特性。

**创新点：** 1. 利用浦东实测基地的测风塔，获得 10 m、20 m、30 m 和 40 m 高度处台风“米雷”的风速实测数据。2. 对台风“米雷”作用下的近地风特性进行分析，并对不同风特性参数之间的相互关系进行研究。

**方　法：** 1. 在浦东实测基地建立 40 m 高的测风塔，利用现场实测的方法，研究台风“米雷”作用下的近地层风场特性；2. 利用经验公式拟合的方法，将现场实测结果与经验公式所得结果进行比较，并分析它们之间的差异。

**结　论：** 1. 各向湍流积分尺度均呈现随平均风速的增大而增大的趋势，在 10 m、20 m 和 40 m 高度处各向湍流积分尺度的均值之比分别为 1∶0.69∶0.08、1∶0.61∶0.09 和 1∶0.65∶0.13；2. 当平均时距大于 10 min 时，$u$ 和 $v$ 方向的湍流积分尺度随平均时距的增大而增大，但 $w$ 方向的湍流积分尺度基本不随平均时距的改变而改变；3. 台风初期惯性子区各湍流分量功率谱的分布斜率小于−5/3，随后逐渐满足 Kolmogorov 5/3 率，纵向脉动风速功率谱与 von Karman 经验谱吻合较好，而横向和竖向脉动风速功率谱与 von Karman 经验谱在高频段有所偏差。

**关键词：** 台风“米雷”；现场实测；湍流积分尺度；衰减系数；功率谱